Allocation of fast-acting energy storage systems in transmission grids with high renewable generation

Allocation of Fast-Acting Energy Storage Systems in Transmission Grids with High Renewable Generation

Ahmad Nikoobakht, Jamshid Aghaei, *Senior Member, IEEE,* Miadreza Shafie-khah, *Senior Member, IEEE,* and João P. S. Catalão, *Senior Member, IEEE*

***Abstract*—The major challenge in coordinating between fast-acting energy storage systems (FA-ESSs) and renewable energy sources (RESs) in the existing transmission grid is to determine the location and capacity of the FA-ESS in the power systems. The optimal allocation of FA-ESS with conventional hourly discrete time method (DTM) can result in the increased operation cost, non-optimal placements and larger storage capacity and therefore, having an opposite effect on the operation. Accordingly, in this paper, a continuous-time method (CTM) is proposed to coordinate FA-ESS and RESs to cover fast fluctuations of renewable generations (RGs). Besides, based on the CTM, an adaptive interval-based robust optimization framework, to deal with uncertainty of the RGs, has been proposed. The proposed optimal allocation of FA-ESS with CTM provides the best sitting and sizing for the installation of the FA-ESSs and the best possible continuous-time scheduling plan for FA-ESSs. Also, in other to have better implementations of their ramping capability to track the continuous-time changes and deviations of the RGs rather than hourly DTM. The proposed model has been implemented and evaluated on the IEEE Reliability Test System (IEEE-RTS).**

***Index Terms*—Renewable energy sources, continuous-time, energy storage systems, robust optimization.**

I. Notation

A. Indices

j	Index of Bernstein basis Function.
w, g, e	Index for generation units, wind farms and ESU, respectively.
n, m	Indexes of buses.
t	Index of continues-time.
κ	Index of time interval.
k	Index of transmission line.
$(\bullet)^{\pm}$	Related to wind uncertainty realization, where '±': '–' and '+' refer to the lower and upper bounds of wind uncertainty range, respectively.
$(\bullet)_{(\cdot),t}$	Related to element $(\cdot)$ at time period t.

All variables and constants include subscript ± and t referring to scenario ± and hour t.

B. Parameters

c_g	Cost of generating unit g.
c_n	Cost of power charge and discharge for FA-ESS.
$P_g^{\max} / P_g^{\min}$	Max/min generation of generating unit g.
$r_g^{\max} / r_g^{\min}$	Max/min ramp rate for generating unit g.
$P_{f,wt} / d_{nt}$	Forecasted wind power/load.
b_k	Transmission line susceptance for line k.
$P_k^{\max}$	Maximum power flow capacity of line k.
η_n^c / η_n^d	Cycle charging/discharging efficiency of FA-ESS at bus n.
$\bar{P}_n^c / \bar{P}_n^d$	Maximum power charging/discharging for FA-ESS at bus n.
$E_n^{\max} / E_n^{\min}$	Max/min net energy capacity for FA-ESS at bus n.
ρ_n	Factor associated with the power charging and discharging of FA-ESS at bus n.
$\Delta\Upsilon_g^{\max}$	Ramp up/down limit of a generating unit g at wind uncertainty realization condition
x_n	Annualized investment cost of the FA-ESS at bus n.
$b_{j,J}^t$	Bernstein basis function of order J.
$\Psi_{J_\kappa}^{f_t}$	Bernstein polynomial operator takes a function f_t.
$C_{j_\kappa}^{(\bullet)}$	Bernstein coefficient of $(\bullet)$.
J	Order of Bernstein polynomial
K	Large enough constant.
ξ	Weighting parameter of uncertainty.
Π	Investment budget for new FA-ESS

C. Variables

P_{gt}	Power generation of generating unit g.
P_{nt}^c / P_{nt}^d	Power charging/discharging of FA-ESS at bus n.
λ_n	Sizing coefficient of FA-ESS at bus n.
I_n	Binary variable that equals 1 if the FA-ESS is installed at bus n, and 0 otherwise.
$\dot{P}_{gt}$	Ramp rate for generating unit g.
ϑ	The variation range of wind uncertainty.
P_{kt}	Power flow on transmission line k.
δ_{nt}	Voltage angle at bus n.
E_{nt}	State of charge for FA-ESS at bus n.
C^{Inv} / C^{Oper}	Investment and operation costs.
$\vec{C}_{J_\kappa}^{(\bullet)}$	Vector containing Bernstein coefficients of $(\bullet)$.
Φ	Total cost.
W_t	Wind power function.

II. Introduction

Installed renewable energy sources, in particular wind energy generation (WEG), have been increased substantially over the last decade. In China for example, the installed WEG capacity extended to 62 GW via the end of 2011 and is planned to the extent of 100 GW via the end of 2015 [1]. Nevertheless, the intermittent characteristics of WEG increase the uncertainty and the fluctuation at power system. Once WEG makes up a large proportion of the committed conventional thermal generating units (TGUs), the minimum load problems can arise once TGUs cannot operate at a much reduced generation or cannot be turned off. Also, the intermittency of WEG usually requires the provision of additional ramping capacity by the conventional TGUs. Fast fluctuations of the generation of particular high penetration of WEG are a substantial issue because usually the fast fluctuations cannot be covered by conventional TGUs. High penetration of WEGs will necessitate more operating reserves leading to higher costs of ancillary services. Also, lack of enough ramp capabilities of conventional TGUs will make hard the compensation of fast variations of WEGs in a short time.

Because of the fast-ramping and charging-discharging capabilities of flexible fast-acting energy storage systems (FA-ESSs), especially battery energy storage system (BESS) or pump storage systems with high ramping capability, can mitigate the fast wind energy fluctuations. The allocation of FA-ESS may defer significant investments on new facilities through peak amend, which mitigates transmission bottlenecks and removes the need for new peaking gas-fired power plants, and providing fast-response ancillary services, improving fast variations of WEG following, facilitating load shifting as well as improving power quality and service reliability. The FA-ESSs can buffer the output of intermittent WEG by providing fast-ramping energy services. Accordingly, it is vital to increase the expansion investments in FA-ESSs in the power systems with a high share of WEGs, with limited ramping capacity [2] and [3].

Since, the investment in FA-ESS requires high monetary assets, accordingly optimization model for siting and sizing of this flexibility sources is vital to cover inherent uncertainty and fast sub-hourly fluctuations of WEG integrated power systems. To deal with uncertainty, three traditional uncertainty modeling approaches are available in electric power systems: (i) stochastic optimization (SO), [4] and [5], and (ii) standard robust optimization (SRO) [6], (iii) proposed interval based robust optimization (IBRO), [7]. In the SO, a large number of scenarios is required to cover more uncertainty spectrum which results in a high computational burden for the large-scale systems [4].

The uncertainty modeling in the proposed IBRO method is similar to that of the SRO method with the difference that in SRO method, it is needed to know the range of the uncertainty and the lower and upper bounds of the uncertainty spectrum are fixed before solving the problem. But, in the IBRO method, the range of the uncertainty spectrum is optimized to have a robust optimal solution for the maximized range of the uncertainty.

Note that, as an advantage for the IBRO method, the application of this method for the proposed problem is much simpler than the SRO and SO methods.

The other advantage of the proposed method is its tractability and simplicity, and hence, the problem sustains in a reasonable size.

Numerous studies are available in the technical literature regarding WEG uncertainty management by the allocation of EESs in transmission grids with significant wind power integrations. In recent studies, the SO and SRO have been employed to solve the joint FA-ESSs placement problem ([8], [9], [10], [11], [12] and [13]). However, the optimal allocation of FA-EES problem with IBRO method in the power system has not been tackled yet. In [5], a stochastic problem based on the substantial number of scenarios has been proposed to determine the optimal sizing of ESSs in a power system with wind uncertainty. In [9], a deterministic optimal allocation EESs is suggested for transmission grids to determine the optimal size and location of ESSs to optimize the use of renewables while reducing the operation costs. References [5] and [12] propose a SO model to coordinate the long-term planning of both ESSs and transmission lines to integrate wind power efficiently. Optimal sizing and siting decisions for the battery ESS is achieved through a deterministic method in [9], which aims at maximizing the system planning and operation cost savings under high renewable penetrations. In [14], an expansion model of ESSs and transmission lines using SRO is proposed. The uncertainty is represented via confidence bounds.

In [15], the transmission network expansion planning is solved considering uncertain dynamic thermal rating of overhead lines. The uncertainties in this paper have been modelled by SO. Noted that, the FA-ESS planning has been not considered by [15].

The co-planning of TEP and ESS has been used in [5]. Must be remembered, this study uses the SM to model wind uncertainty.

Recent research on ROM for solving the TEP is reported in [16] and [17]. The uncertainty considered is represented via confidence bounds. Noted that, the ESS planning has been not parented by [16] and [17]. On the other hand, in [12], a planning problem of ESS and transmission using ROM is proposed.

In the above research works [8]–[17], the hourly discrete-time method (DTM) has been used in the optimal operation of ESSs with fast fluctuations of WEG. However, the current hourly discrete-time method for operation of ESSs by sampling the demand hourly and having hourly decision variables for charging/discharging, the hourly unit commitment status and generation schedule, has functioned satisfactorily to handle the uncertainty and variability of load. However, this method is unable to deal with the fast sub-hourly variations to the system due to increasing integration of WEGs. Indeed, sub-hourly variations lead to frequent occurrence of large deficits or excesses for ESS capacity (or non-optimal allocation of ESSs). Also, the current hourly DTM in the proposed problem does not efficiently employ the existing ramping capability of FA-ESSs to better capture the fast sub-hourly ramping of WEG.

On the other hand, the actual real-time WEG can be divided to the discrete-time intervals that needs to be absorbed by the power system at the subsequent stages of operation, depending to different independent system operators (ISOs) market structure. The discrete-time

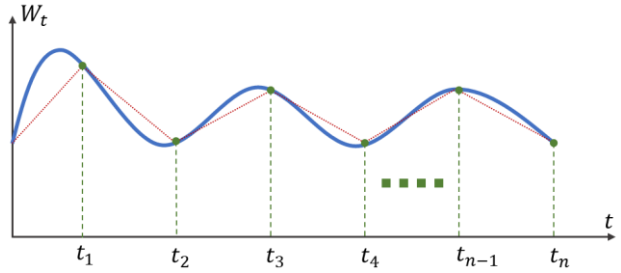

Fig. 1. Linear spline approximation of the continuous wind power profile.

intervals deviation results from two kinds of error in system operation: 1) error due to the imperfect sub-hourly interval forecast, 2) error due to the wind power profile approximation. Here, we argue that the ramping scarcity problems are originated, partly, due to the inherent error in the current practice of sub-hourly interval wind power profile approximation. In fact, ramping events and constraints are inter-temporal continuous-time mathematical objects. The natural implication of the current discrete-time formulation is that, within the hour or minutes intervals, generators shall follow a linear ramp from one value to the next. Habitually, looking at Fig. 1, the linear trajectory does not fully capture the prior information about sub-hourly variations of the wind power and one must expect deviation which will have to be handled in the real-time operation. If this short-term deviation is beyond the coverage of the hourly operation decisions, the short-term operations may be left with sufficient capacity but without ramping capability to respond to sub-hourly WEG variations, as was observed by multiple ISOs [18], with obviously undesirable economic and security consequences. These observations demonstrate that the current discrete-time model does not efficiently utilize the available ramping capability of the FA-ESS and the prior information about the WEG.

Accordingly, in this paper a continuous-time method based on coefficients of Bernstein polynomial is proposed which allows to better schedule the ramping capability of FA-ESSs and TGUs while it provides a more accurate representation of the sub-hourly ramping needs to follow fast sub-hourly ramping of WEG. Also, the application of continuous-time method (CTM) in our proposed problem would modify the investment and operation costs and would utilize FA-ESS and TGU in such that the coordination of FA-ESS and online units is better arranged to coverage of sub-hourly deviations of the WEG and load in the real-time operation.

All the literature cited above are not successful enough in taking the continuous time nature of some actions into account, such as sub-hourly variations of WEG and ramping needs. Undoubtedly, the allocation of FA-ESS with DTM can cause non-optimal location and/or capacity for FA-ESS that it does not appropriately coordinate with the flexibility of TGUs to compensate the faster variations of WEG leading to the happenings of ramping shortages.

Finally, taking the above description about the available literature into consideration, to the best of authors' knowledge the contributions of this paper are twofold:

- This paper has proposed a robust continuous-time optimal allocation of FA-ESSs model to determine the optimal location and capacity for FA-ESSs.
- In this paper a CTM is utilized to capture the fast response of FA-ESS to supply the fast ramping requirements of sub-hourly ramping of WPGs. Also, the continuous-time method modifies the coordination of TGUs and FA-ESSs, in such a way that the configuration of online TGUs and FA-ESSs is better set to react the sub-hourly ramping requirement of operation.
- An IBRO approach is employed to minimize operation cost against the undesired effects of fast sub-hourly variations of WEG.

TABLE I: Taxonomy of the proposed planning problem in current paper (CP).

Ref	Year	Storage Planning	Continuous Time Model	Wind uncertainty	IBRO method
[2]	2013	Y	N	Y	N
[8]	2018	Y	N	Y	N
[19]	2019	Y	N	Y	N
[20]	2016	Y	N	N	N
[21]	2017	N	N	Y	N
[15]	2019	N	N	Y	N
[22]	2016	Y	N	Y	N
[23]	2019	N	N	Y	Y
CP	N	Y	Y	Y	Y

Y/N denotes that the subject is/is not considered.

As shown in Table 1, except current paper, no reference in the literature, which was published in recent years, proposes a continuous-time model for optimal allocation of FA-ESSs in power systems.

Must be remembered, Table 1 compares the proposed methods which has been presented in this paper with other methods in previous studies to highlight the paper contributions.

The remainder of this paper is organized as follows. Section III problem formulation. Section IV continuous-time modeling. Section IV case study. Finally, Section VII concludes.

III. Proposed Planning Model

A. Model Structure

The structure of the proposed model is shown in Fig. 2. The planning problem seeks the optimal size and location for FA-ESS, with minimum investment /operational costs and maximum wind power uncertainty.

As shown in Fig. 2, the proposed problem has two stage constraints. In first constraints optimal output of TGUs, number/size/location for FA-ESS, investment/operation costs are determined by ISO. Also, in second stage constraints worse-case uncertainty for WEG is specified.

B. Problem formulation

The detailed formulation of original continuous-time optimal allocation of FA-ESS problem is provided below:

$$min \quad \Phi = \overbrace{\sum_{n\in\Omega_n} x_n\lambda_n}^{C^{Inv}} + \overbrace{\sum_g\left(\int_T (c_g P_{gt})dt\right) + \sum_{n\in\Omega_n}\left(\int_T c_n(P_{nt}^c + P_{nt}^d)dt\right)}^{C^{Oper}} \tag{1a}$$

s.t.

$$\sum_n x_n\lambda_n \le \Pi \tag{1b}$$

$$0 \le x_n\lambda_n \le \mathrm{K} I_n \tag{1c}$$

$$I_n \le \lambda_n \tag{1d}$$

$$P_g^{\min} \le P_{gt} \le P_g^{\max} \tag{1e}$$

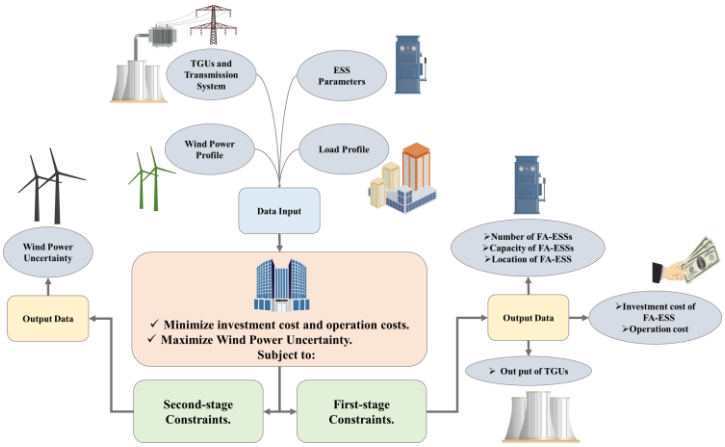

Fig. 2. Structure of the proposed model.

$$r_g^{\min} \le \frac{dP_{gt}}{dt} = \dot{P}_{gt} \le r_g^{\max} \tag{1f}$$

$$-P_k^{\max} \le P_{kt} = b_{nm} \cdot \left(\delta_{nt} - \delta_{mt}\right) \le P_k^{\max} \tag{1g}$$

$$\sum_{g(n)} P_{gt} + \sum_{w(n)} P_{f,wt} + \sum_{n} P_{nt}^{d} - \sum_{k(n,m)} P_{kt} + \sum_{k(m,n)} P_{kt} = d_{nt} + \sum_{e(n)} P_{nt}^{c} \tag{1h}$$

$$\frac{dE_{nt}}{dt} = \eta^{c} P_{nt}^{c} - \frac{P_{nt}^{d}}{\eta^{d}} \tag{1i}$$

$$\int_{T} \left(\eta^{c} P_{nt}^{c} - \frac{P_{nt}^{d}}{\eta^{d}} \right) = 0 \tag{1j}$$

$$0 \le P_{nt}^{c} \le \bar{P}_{n}^{c} \lambda_n \rho_n \tag{1k}$$

$$0 \le P_{nt}^{d} \le \bar{P}_{n}^{d} \lambda_n \rho_n \tag{1l}$$

$$E_n^{\min} \lambda_n \le E_{nt} \le E_n^{\max} \lambda_n \tag{1m}$$

$$P_{g,t=0} = P_g^0, \; E_{n,t=0} = E_n^0 \tag{1n}$$

The objective function (1a) represents the total cost, which includes the investment cost of FA-ESSs and the operation cost. The investment cost refers to the building of new FA-ESS. The operation cost includes operation cost of TGUs and power charging/discharging of FA-ESSs. Constraint (1b) ensures the investment cost of FA-ESSs does not surpass its available investment budget. Note that if I_n for nth bus equals 0 then the investment cost of FA-ESS at this bus equals zero, which is denoted by (1c), and also, (1d) with (1c) guarantees that once I_n equals 1, the capacity factor for FA-ESS at nth bus is greater than one and once I_n equals 0 the capacity factor is 0. Constraint (1e) is the generation limits for TGUs. Constraint (1f) is the continuous-time ramping up and down of TGUs. Noted that, the associated ramping of TGUs is defined as time derivatives of the generation of TGUs. Constraint (1g) warrants the lower and upper limits of the DC power flow in line k. Constraint (1h) denotes the continues-time power balance equation.

The constraint (1i) controls the state of charge of FA-ESSs in continuous-time over the operation horizon; η^c / η^d in (1i) is charging/discharging efficiency, respectively. Constraint (1j) imposes energy balance for the FA-ESSs per day. Constraints (1k) and (1l) are charging and discharging power limits for FA-ESS at bus n. Constraint (1m) defines the min and max energy storage levels for the FA-ESS at bus n. Initial values of the state routes are enforced by (1n), where P_g^0, and E_e^0 are the vectors of constant initial values.

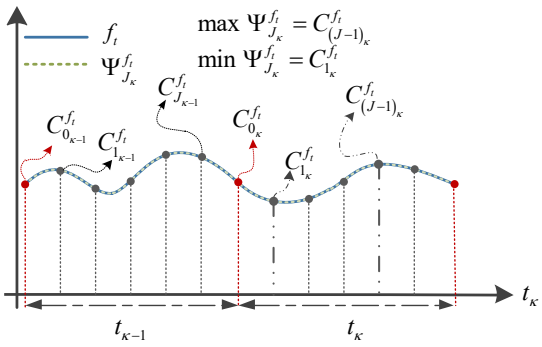

Fig.3. The Bernstein coefficients for f_t.

IV. Continuous-Time Modeling

Here Bernstein polynomial of order J has been deployed to approximate the continuous-time trajectory (space) of a function or a data set with the given level of the accuracy. The Bernstein polynomial has the capability to approximate complex functions or data sets through curve fitting and interactive curve design [24]. One advantage of using polynomials is that they can be calculated very quickly on a computer. Here, the vector of polynomials of degree J is defined as b_J^t:

$$b_{j,J}^{t} = \binom{J}{j} t^{j} (1-t)^{J-j} \tag{2a}$$

If the function f_t is continuous on $t \in [0,1]$, the Bernstein polynomial operator $\Psi_J^{(\cdot)}$ takes this function and maps it into a Jth order polynomial as

$$\Psi_{J_\kappa}^{f_t} = \sum_{j_k=0}^{J_\kappa} C_{j_\kappa}^{f_t} \cdot b_{j,J}^{t} \tag{2b}$$

The coefficients $C_{j_\kappa}^{f_t}$ are called control points (as shown in Fig.3). The other useful properties of BPs are as follows:

(i) When the order J for Bernstein polynomial operator is increased, the approximation error will be reduced, i.e., $\lim_{J_\kappa \to \infty} \Psi_{J_\kappa}^{f_t} = f_t$.

(ii) The derivative of $\Psi_{J_\kappa}^{f_t}$ can be written as a combination of two polynomials of lower degree $J_\kappa - 1$.

$$\dot{\Psi}_{(J-1)_\kappa}^{f_t} = J_\kappa \sum_{j_\kappa=0}^{J_\kappa - 1} \left(C_{j_\kappa}^{f_t} - C_{(j-1)_\kappa}^{f_t} \right) b_{j_\kappa,(J-1)_\kappa}^{t} \tag{2c}$$

(iii) Integrating $\Psi_{J_\kappa}^{f_t}$ is given by:

$$\int_{t_\kappa}^{t_{\kappa+1}} \Psi_{J_\kappa}^{f_t} = \int_{t_\kappa}^{t_{\kappa+1}} \left(C_{j_\kappa}^{f_t} \cdot b_{j,J}^{t} \right) dt = \frac{\sum_{j_\kappa}^{J_\kappa} C_{j_\kappa}^{f_t}}{J_\kappa + 1} \tag{2d}$$

(iv) Convex hull property of $b_{j,J}^t$ causes that $\Psi_J^{f_t}$ and $\dot{\Psi}_J^{f_t}$ are limited between their max and min coefficients (as shown in Fig.3).

$$\min_{\forall j_\kappa} \left\{ C_{j_\kappa}^{f_t} \right\} \le \Psi_{J_\kappa}^{f_t} \le \max_{\forall j_\kappa} \left\{ C_{j_\kappa}^{f_t} \right\} \tag{2e}$$

$$\min_{\forall j_\kappa} \left\{ C_{j_\kappa}^{f_t} - C_{(j-1)_\kappa}^{f_t} \right\} \le \dot{\Psi}_{(J-1)_\kappa}^{f_t} \le \max_{\forall j_\kappa} \left\{ C_{j_\kappa}^{f_t} - C_{(j-1)_\kappa}^{f_t} \right\} \tag{2f}$$

These properties significantly help later, when max and min generations and ramping constraints are driven.

(iv) In order to maintain continuity across first and end points of function f_t, it is sufficient to enforce that the control points match at the first and end points.

$$C^{f_t}_{(0)_\kappa} = C^{f_t}_{J_{\kappa-1}} \tag{2g}$$

Also, the differential of $\Psi^{f_t}_{J_\kappa}$ should also be continuous.

$$C^{f_t}_{1_\kappa} - C^{f_t}_{(0)_\kappa} = C^{f_t}_{J_{\kappa-1}} - C^{f_t}_{(J-1)_{\kappa-1}} \tag{2h}$$

These properties significantly help later, to maintain generation and ramping continuity for TGUs, respectively. In the following, continuous-time approximation of wind power and load profiles and equations (1) are modeled based on the above-mentioned Bernstein polynomials method.

***A. Load and wind Profiles*:**

- *Load profile approximation*: the continuous-time approximated load profile, similar to Fig. 3, can be addressed by the vector of Bernstein basis functions of degree J in hour t_κ and sub-interval j_κ, i.e., $\left\{b^{t-t_\kappa}_{0_\kappa,J_\kappa}, b^{t-t_\kappa}_{1_\kappa,J_\kappa},..., b^{t-t_\kappa}_{J_\kappa,J_\kappa}\right\}$. Each element of Bernstein basis vector weighted by the value of load at the sub-interval j_κ and at hour t_κ, as follows:

$$\Psi^{D_{n,t}}_{J_\kappa} = \sum_{j_\kappa=0}^{J_\kappa} C^{D_{n,t}}_{j_\kappa} \cdot \binom{J_\kappa}{j_\kappa} \cdot (t-t_\kappa)^j \cdot \left(1-(t-t_\kappa)\right)^{(J-j)_\kappa}, \quad \forall t \in [t_\kappa, t_{\kappa+1}) \tag{3a}$$

To show this equation in matrix form, which is more implementable, it can be divided into the product of Bernstein coefficients and Bernstein basis functions as follows:

$$\Psi^{D_{n,t}}_{J_\kappa} = \begin{bmatrix} C^{D_{n,t}}_{o_\kappa} & C^{D_{n,t}}_{1_\kappa} & \cdots & C^{D_{n,t}}_{J_\kappa} \end{bmatrix} \begin{bmatrix} b^{t-t_\kappa}_{0_\kappa,J_\kappa} \\ b^{t-t_\kappa}_{1_\kappa,J_\kappa} \\ \vdots \\ b^{t-t_\kappa}_{J_\kappa,J_\kappa} \end{bmatrix} = \vec{C}^{D_{n,t}}_{J_\kappa} \vec{b}^{t-t_\kappa}_{J_\kappa} \tag{3b}$$

As mentioned earlier, with a large enough J, the deviation of the main function and its Bernstein approximation will be small.

- *Wind profile approximation*: the continuous-time Wind profile like load profile can be modeled by Bernstein approximation as follows:

$$\Psi^{W_{w,t}}_{J_\kappa} = \vec{C}^{W_{f,wt}}_{J_\kappa} \vec{b}^{t-t_\kappa}_{J_\kappa}, \forall t \in [t_\kappa, t_{\kappa+1}) \tag{3c}$$

Noted that, the vector $\vec{C}^{W_{w,t'}}_{J_\kappa}$ and $\vec{C}^{D_{n,t'}}_{J_\kappa}$ are calculated alike.

***B. The TGU generation*:** the continuous-time TGU generation, $P_{g,t}$, can be defined by the Bernstein function space as:

$$P^{\min}_g \le \Psi^{P_{g,t}}_{J_\kappa} = \vec{C}^{P_{g,t}}_{J_\kappa} \vec{b}^{t-t_\kappa}_{J_\kappa} \le P^{\max}_g, \forall t \in [t_\kappa, t_{\kappa+1}) \tag{3d}$$

The time between t_κ and $t_{\kappa+1}$ has been divided into J arbitrary subintervals and a vector of Bernstein coefficients of TGU generation has been assigned as $\vec{C}^{P_{g,t}}_{J_\kappa} = \left[C^{P_{g,t}}_{0_\kappa,J_\kappa}, C^{P_{g,t}}_{1_\kappa,J_\kappa},..., C^{P_{g,t}}_{J_\kappa,J_\kappa}\right]$ subsequently.

According to (2e) and Fig. 3, the $\Psi^{P_{g,t}}_{J_\kappa}$ should be limited between max and min of Bernstein coefficients of TGU generation or units generation limits.

$$P^{\min}_g \le \vec{C}^{P_{g,t}}_{J_\kappa} \le P^{\max}_g \tag{3e}$$

C. The TGU Ramping limits: According to (2c), the continuous-time ramping limits of TGUs can be modeled as follows:

$$r^{\min}_g \le \dot{\Psi}^{P_{g,t}}_{(J-1)_\kappa} = J_\kappa \vec{C}^{P_{g,t}}_{(J-1)_\kappa} \vec{b}^{t-t_\kappa}_{(J-1)_\kappa} \le r^{\max}_g \tag{3f}$$

$$\vec{C}^{P_{g,t}}_{(J-1)_\kappa} = J_\kappa \left[C^{P_{g,t}}_{1_\kappa,(J-1)_\kappa} - C^{P_{g,t}}_{0_\kappa,(J-1)_\kappa}, \cdots, C^{P_{g,t}}_{(J-1)_\kappa,(J-1)_\kappa} - C^{P_{g,t}}_{(J-2)_\kappa,(J-1)_\kappa}\right] \tag{3g}$$

According to (2f), to put a limitation on the continuous-time ramping of TGUs, the following equation should be satisfied:

$$\frac{r^{\min}_g}{J_\kappa} \le \vec{C}^{P_{g,t}}_{(J-1)_\kappa} \le \frac{r^{\max}_g}{J_\kappa} \tag{3h}$$

E. The power charging/discharging and energy storage limits: Similar to (3d), the power charging and discharging of FA-ESS are modeled, respectively, as follows:

$$0 \le \Psi^{P^c_{n,t}}_{J_\kappa} = \vec{C}^{P^c_{n,t}}_{J_\kappa} \vec{b}^{t-t_\kappa}_{J_\kappa} \le \bar{P}^c_n \lambda_n \rho_n \Rightarrow 0 \le \vec{C}^{P^c_{n,t}}_{J_\kappa} \le \bar{P}^c_n \lambda_n \rho_n \tag{3i}$$

$$0 \le \Psi^{P^d_{n,t}}_{J_\kappa} = \vec{C}^{P^d_{n,t}}_{J_\kappa} \vec{b}^{t-t_\kappa}_{J_\kappa} \le \bar{P}^d_n \lambda_n \rho_n \Rightarrow 0 \le \vec{C}^{P^d_{n,t}}_{J_\kappa} \le \bar{P}^d_n \lambda_n \rho_n \tag{3j}$$

Where $\vec{C}^{P^c_{n,t}}_{J_\kappa} = \left[C^{P^c_{n,t}}_{0_\kappa,J_\kappa},...,C^{P^c_{n,t}}_{J_\kappa,J_\kappa}\right]$ and $\vec{C}^{P^d_{n,t}}_{J_\kappa} = \left[C^{P^d_{n,t}}_{0_\kappa,J_\kappa},..,C^{P^d_{n,t}}_{J_\kappa,J_\kappa}\right]$ are the vectors of Bernstein coefficients of power charging and discharging, respectively. Similarly, the energy storage capacity limits can be modeled by (2k):

$$E^{\min}_n \lambda_n \le \Psi^{E_{n,t}}_{J_\kappa} = \vec{C}^{E_{n,t}}_{J_\kappa} \vec{b}^{t-t_\kappa}_{J_\kappa} \le E^{\min}_n \lambda_n \Rightarrow E^{\min}_n \lambda_n \le \vec{C}^{E_{n,t}}_{J_\kappa} \le E^{\max}_n \lambda_n \tag{3k}$$

***G. The energy storage of FA-ESS*:** By integrating the state equation (1i) over $j-1$ and j, the energy storages of FA-ESS are driven by the Bernstein function space of degree *J*+1. Noted that, the integral of the Bernstein function space of degree *J* are linearly associated with Bernstein function space of degree *J*+1.

$$\int_{j-1}^{j} \frac{dE_{nt}}{dt} = \int_{j-1}^{j} \left(\eta^c P^c_{n,t} - \frac{P^d_{n,t}}{\eta^d}\right) = \int_{j-1}^{j} \frac{d\Psi^{E_{n,t}}_{J_\kappa}}{dt} = \int_{j-1}^{j} \left(\eta^c \Psi^{P^c_{n,t}}_{J_\kappa} - \frac{\Psi^{P^d_{n,t}}_{J_\kappa}}{\eta^d}\right) \tag{3l}$$

$$\Psi^{E_{n,j}}_{(J+1)_\kappa} - \Psi^{E_{n,j-1}}_{(J+1)_\kappa} = \left(\eta^c \Psi^{P^c_{n,j}}_{(J+1)_\kappa} - \frac{\Psi^{P^d_{n,j}}_{(J+1)_\kappa}}{\eta^d}\right) \Rightarrow$$

$$\vec{C}^{E_{n,j}}_{(J+1)_\kappa} \vec{b}^{t-t_\kappa}_{(J+1)_\kappa} - \vec{C}^{E_{n,j-1}}_{(J+1)_\kappa} \vec{b}^{t-t_\kappa}_{(J+1)_\kappa} = \left(\eta^c \left(\vec{C}^{P^c_{n,j}}_{(J+1)_\kappa} \vec{b}^{t-t_\kappa}_{(J+1)_\kappa}\right) - \left(\eta^d\right)^{-1} \left(\vec{C}^{P^d_{n,j}}_{(J+1)_\kappa} \vec{b}^{t-t_\kappa}_{(J+1)_\kappa}\right)\right) \tag{3m}$$

By removing $\vec{b}^{t-t_\kappa}_{(J+1)_\kappa}$ from both sides of the equation (3l), we have:

$$\vec{C}^{E_{n,j}}_{(J+1)_\kappa} - \vec{C}^{E_{n,j-1}}_{(J+1)_\kappa} = \left(\eta^c \left(\vec{C}^{P^c_{n,j}}_{(J+1)_\kappa}\right) - \left(\eta^d\right)^{-1} \left(\vec{C}^{P^d_{n,j}}_{(J+1)_\kappa}\right)\right) \tag{3n}$$

***H. The power flow equations*:** By substituting the Bernstein models of line flow and voltage angle in equation (1g), we derive:

$$\begin{cases} \Psi^{P_{kt}}_{J_\kappa} = b_{nm} \cdot \left(\Psi^{\delta_{n,t}}_{J_\kappa} - \Psi^{\delta_{m,t}}_{J_\kappa}\right) \Rightarrow \vec{C}^{P_{kt}}_{J_\kappa} = b_{nm} \cdot \left(\vec{C}^{\delta_{n,t}}_{J_\kappa} - \vec{C}^{\delta_{m,t}}_{J_\kappa}\right) \\ \Psi^{P_{kt}}_{J_\kappa} = \vec{C}^{P_{kt}}_{J_\kappa} \vec{b}^{t-t_\kappa}_{J_\kappa}, \quad \Psi^{\delta_{n,t}}_{J_\kappa} = \vec{C}^{\delta_{n,t}}_{J_\kappa} \vec{b}^{t-t_\kappa}_{J_\kappa} \end{cases} \tag{3o}$$

Then, the continuous-time limits on the line flow can be imposed via limitation on the vector of Bernstein coefficients, i.e., (3p).

$$-P^{\max}_k \le \vec{C}^{P_{kt}}_{J_\kappa} \le P^{\max}_k \tag{3p}$$

***I. The nodal Balance equation*:** By substituting the Bernstein models of load from (3b), WEG from (3c), TGU generation from (3d), power charging and discharging of FA-ESS from (3i) and (3j), respectively and line flow from

(3o) in the continuous-time power balance constraint (1h), we have:

$$\sum_{g(n)} \vec{C}^{P_{g,t}}_{J_\kappa} \vec{b}^{t-t_\kappa}_{J_\kappa} + \sum_{w(n)} \vec{C}^{W_{f,wt}}_{J_\kappa} \vec{b}^{t-t_\kappa}_{J_\kappa} + \sum_{n} \vec{C}^{P^d_{n,t}}_{J_\kappa} \vec{b}^{t-t_\kappa}_{J_\kappa} - \sum_{k(n,m)} \vec{C}^{P_{kt}}_{J_\kappa} \vec{b}^{t-t_\kappa}_{J_\kappa} + \sum_{k(m,n)} \vec{C}^{P_{kt}}_{J_\kappa} \vec{b}^{t-t_\kappa}_{J_\kappa} = \vec{C}^{d_{n,t_\kappa}}_{J_\kappa} \vec{b}^{t-t'}_{J_\kappa} + \sum_{n} \vec{C}^{P^c_{n,t}}_{J_\kappa} \vec{b}^{t-t_\kappa}_{J_\kappa} \quad (3q)$$

By removing $\vec{b}^{t-t_\kappa}_{J_\kappa}$ from both sides of the equation (3q), we have:

$$\sum_{g(n)} \vec{C}^{P_{g,t}}_{J_\kappa} + \sum_{w(n)} \vec{C}^{W_{f,wt}}_{J_\kappa} + \sum_{n} \vec{C}^{P^d_{n,t}}_{J_\kappa} - \sum_{k(n,m)} \vec{C}^{P_{kt}}_{J_\kappa} + \sum_{k(m,n)} \vec{C}^{P_{kt}}_{J_\kappa} = \vec{C}^{d_{n,t_\kappa}}_{J_\kappa} + \sum_{n} \vec{C}^{P^c_{n,t}}_{J_\kappa} \quad (3r)$$

Equation (3r) converts the continuous-time nodal balance equation (1h) to algebraic equations on the Bernstein coefficients like traditional discrete-time nodal balance equation.

***J. power generation (charging/discharging) continuity*:** According to (2g), the continuity of power generation of TGU and power charging (discharging) of FA-ESS at the intersection of hourly intervals are modeled as follows:

$$\left\{ C^{P_{g,t}}_{0_\kappa,J_\kappa} = C^{P_{g,t}}_{J_{\kappa-1},J_{\kappa-1}}, C^{P^d_{n,t}}_{0_\kappa,J_\kappa} = C^{P^d_{n,t}}_{J_{\kappa-1},J_{\kappa-1}}, C^{P^c_{n,t}}_{0_\kappa,J_\kappa} = C^{P^c_{n,t}}_{J_{\kappa-1},J_{\kappa-1}} \right\} \quad (3s)$$

K. Ramping Continuity: For TGU, it is physically impossible to have instantaneous changes in ramping. According to (2h), this constraint can be achieved by (3t):

$$C^{P_{g,t}}_{1_\kappa,J_\kappa} - C^{P_{g,t}}_{0_\kappa,J_\kappa} = C^{P_{g,t}}_{J_{\kappa-1},J_{\kappa-1}} - C^{P_{g,t}}_{(J-1)_{\kappa-1},J_{\kappa-1}} \quad (3t)$$

***K. Investment and operation costs*:** According to (2d), the objective (1a) can be converted to (3u).

$$\min \Phi = C^{Inv} + \sum_g \left(\sum_\kappa \frac{c_g \sum_{j_k=0}^{J_k} C^{P_{g,t}}_{j_\kappa,J_\kappa}}{J_\kappa + 1} \right) + \sum_n \left(\sum_\kappa \frac{c_g \sum_{j_\kappa=0}^{J_\kappa} \left(C^{P^c_{n,t}}_{j_\kappa,J_\kappa} + C^{P^d_{n,t}}_{j_\kappa,J_\kappa} \right)}{J_\kappa + 1} \right) \quad (3u)$$

V. Continuous-time Robust Placement of FA-ESS

To derive the proposed continuous-time robust optimization problem, we want to achieve the largest variation range of wind uncertainty that the system can remain feasible under minimum investment cost (IC) and operation cost (OC).

Accordingly, the proposed robust problem has two-stage constraints, the first stage constraints correspond to the optimal decision for the base case (before the realization of the uncertainties), while the second stage constraints correspond to the optimal decision for post uncertainty realization which can be formulated as follows:

$$\min \quad \Phi + \xi \cdot \vartheta \quad (4a)$$

The first-stage constraints are:

$$(3e),\ (3h),\ (3i)-(3j),\ (3k),\ (3n),\ (3p),\ (3r)-(3s),\ (3t)\ and\ (3u) \quad (4b)$$

The second-stage constraints are:

$$\sum_{g(n)} \vec{C}^{P^{\pm}_{g,t}}_{J_\kappa} + \sum_{w(n)} (1 \pm \vartheta) \vec{C}^{W_{f,wt}}_{J_\kappa} + \sum_{n} \vec{C}^{P^{d^{\pm}}_{n,t}}_{J_\kappa} - \sum_{k(n,m)} \vec{C}^{P^{\pm}_{kt}}_{J_\kappa} + \sum_{k(m,n)} \vec{C}^{P^{\pm}_{kt}}_{J_\kappa} = \vec{C}^{d_{n,t_\kappa}}_{J_\kappa} + \sum_{n} \vec{C}^{P^{d^{\pm}}_{n,t}}_{J_\kappa} \quad (4c)$$

$$\left| \vec{C}^{P_{g,t}}_{J_\kappa} - \vec{C}^{P^{\pm}_{g,t}}_{J_\kappa} \right| \le \Delta \Upsilon^{\max}_g \quad (4d)$$

$$(3e),\ (3h),\ (3i),(3j),\ (3k),\ (3n),\ (3p),\ (3s),\ (3t)\ and\ (3u) \quad (4e)$$

The objective function (4a) represents the continuous-time investment and operation costs plus the largest variation range of the wind uncertainty. Also, the weighting parameter of uncertainty $\xi \in [0, \infty)$ in the objective function (4a) is a weighting parameter used to materialize the tradeoff between total cost and wind uncertainty variation range. If $\xi = 0$, the wind uncertainty term in the objective function is neglected and the resulting problem becomes the uncertainty neutral one. As ξ increases, the total cost becomes less significant with respect to the uncertainty term. The nodal balance (4c) is similar to (3r) but it is related to the wind uncertainty conditions. The changes in the sub-hourly power output of TGUs under wind uncertainty condition is limited by ramp constraint (4d). Constraints in (4e) are similar to (3e), (3h), (3i), (3j), (3k), (3n), (3p), (3s), (3t) and (3u) while considering the wind uncertainty conditions, where the vector of Bernstein coefficients $\vec{C}^{P_{g,t}}_{J_\kappa}$, $\vec{C}^{P^c_{n,t}}_{J_\kappa}$, $\vec{C}^{P^d_{n,t}}_{J_\kappa}$, $\vec{C}^{E_{n,j}}_{(J+1)_\kappa}$, $\vec{C}^{P^{\pm}_{kt}}_{J_\kappa}$, $\vec{C}^{E_{n,t}}_{J_\kappa}$ and $\vec{C}^{\delta_{n,t}}_{J_\kappa}$ are replaced by $\vec{C}^{P^{\pm}_{g,t}}_{J_\kappa}$ $\vec{C}^{P^{c^{\pm}}_{n,t}}_{J_\kappa}$, $\vec{C}^{P^{d^{\pm}}_{n,t}}_{J_\kappa}$, $\vec{C}^{E^{\pm}_{n,j}}_{(J+1)_\kappa}$, $\vec{C}^{P^{\pm}_{kt}}_{J_\kappa}$, $\vec{C}^{f^{\pm}_{k,t}}_{J_\kappa}$, $\vec{C}^{E^{\pm}_{n,t}}_{J_\kappa}$ and $\vec{C}^{\delta^{\pm}_{n,t}}_{J_\kappa}$, respectively. Also, '±' in constraints (4): '-' and '+' refer to the lower and upper margins of possible wind power uncertainty, respectively. The optimal solution obtained from solving the proposed robust problem (4) depends on the value of the weighting parameter of uncertainty (ξ). For instance, for a small value of ξ, it yields a low conservative (or robustness) solution and also a low total cost. In contrast, a large value of ξ achieves a solution with a high conservative solution and also high total cost. Finally, the robustness metric is achieved by comparing the largest variation range of the wind uncertainty with the target range of its uncertainty.

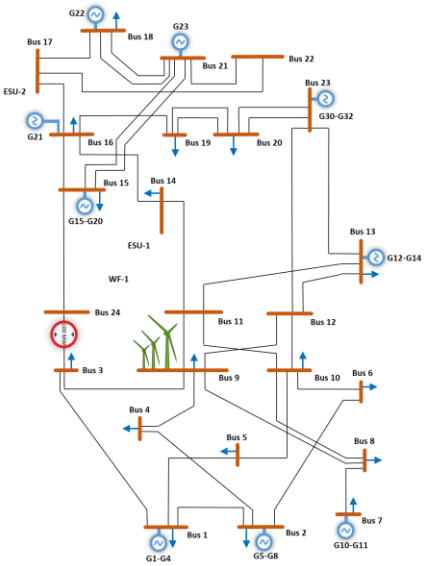

Fig. 4. One-line diagram of the 24-bus RTS.

VI. Case Study

In this section the numerical results to find the optimal location of FA-ESS with a continues-time robust method are based on the one-area 24-bus reliability test system [25] and this system has been modified according to [5]. As shown in Fig.4, the mentioned test system has 26 TGUs, one wind farm (WF), 17 demands and 38 lines. The WF has been installed on bus 9 with the capacity of 900 MW. Three typical load levels with 48-hour periods representing loads in three seasons have been evaluated; the time periods are the fifth and sixth day of the 11th, 25th, and 51st weeks in the year. The fifth and sixth day of the week (Friday and Saturday) have been selected since they denote both lower load levels on weekends and higher load levels during weekdays. 11th, 25th, and 51st weeks have their place to spring, summer and winter, respectively. Level of loads in the fall and spring are very alike, thus they can be considered via the spring load levels as well. The load factor data are given in [25], as shown in this reference the load factors in winter is the highest in overall. Accordingly, the continues-time and hourly discrete-time load factors for the three selected periods are given in Fig. 5 (a). Similarly, the continues-time and discrete-time wind power output for the fifth and sixth days of the 11th, 25th, and 51st weeks in the year is obtained from the Wind Integration Datasets of National Renewable Energy Laboratory (NREL) [26] and shown in Fig.5 (b).

The available FA-ESSs have been considered to be in multiples of 32 MWh basic storage capacity, with the maximum charge and discharge rates per hour set at ρ_n = 25% of this capacity. The power charging and discharging efficiencies are considered to be 90% each. All buses have been considered to be candidates for installing FA-ESS. Also, here assumes that FA-ESS has very high ramping capability. The Bernstein polynomial of degree 3 is implemented to simulate the proposed continues-time method (CTM). The simulations have been implemented on a PC with 4.2-GHz quad-core Intel Core i7 processor with 16 GB of RAM.

The computation times for the proposed planning problem based on DTM and CTM are 5 min, and 12 min, respectively. The increase in the computational time of CTM is expected while the number of continuous variables is increased in this model. This means that the computational time for CTM may significantly increase if a comparatively larger system is considered.

However, to tackle case studies pertaining to real-world systems with thousands of nodes and lines and a large number of FA-ESS, the following additional alternatives are also available:

- To use a supercomputer.
- To implement parallelization techniques.
- To apply decomposition techniques to decompose the problem and/or to reduce the number of new FA-ESS.
- To decompose the network by area [27].

A. Optimal Allocation of FA-ESS, for DTM and CTM, versus Weighting Parameter of Uncertainty: Given Π = 20 M$, the IC and OC for optimal allocation of FA-ESS, for discrete-time and continues-time methods, under different values of ξ are shown in Tables II and III. The IC and OC for both methods are increased by varying the value of ξ from 0 to 10^8. The main reason is that increasing

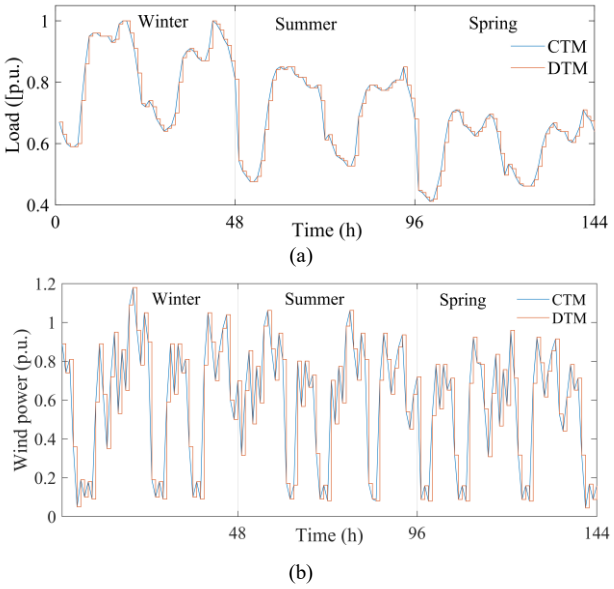

Fig.5. a) Load profile and b) Wind power profile model for CTM and DTM.

the value of ξ results in more conservative allocation of FA-ESS, which can withstand the worst case realizations of WEG uncertainty. Accordingly, both operation and investment costs have been increased which is indeed the price of robustness of more conservative allocation of FA-ESS. Also, as shown in Tables II and III, if ξ = 0, the uncertainty term in the objective function is ignored and the resulting proposed problem for both methods becomes the deterministic one with $\vartheta = 0$. In this condition, from Tables II and III it can be observed that the number of installed FA-ESS for both methods are alike, but, their locations and capacities are different.

For example, for the DTM, any FA-ESS has not been installed at bus 9 (wind farm location), in this condition, the variability of WEG at bus 9 can only be compensated by FA-ESS in other buses i.e., bus 3. But, for the CTM, an FA-ESS with capacity 288 MWh is installed at bus 9 to mitigate the variability of WEG by charging once WEG is high and discharging when WEG is low. Also, the IC in the CTM is higher than it in DTM, but, the decrease in OC for CTM is large enough to offset the IC. This can happen because in the CTM, more energy storage capacity is allocated in the system. Hence, the total cost (Φ) for CTM has more decrease with respect to the DTM. These results are summarized in the first row of Tables II and III. Similarly, when the parameter ξ is 10^6, the number of FA-ESSs is increased to 5 and 6, for DTM and CTM, respectively. Accordingly, the increase of IC in the CTM is higher than the DTM, while, the increase of OC in the CTM is smaller than the DTM. This finding is expected, because the more installation of the storage system leads to a more smoothness of the variation of wind energy results in a significant decrease in the OC. The impact of the ξ value on the worst-case realization of WEG uncertainty (ϑ), for both methods, is illustrated in Tables II and III. As expected, the ϑ value keeps increasing as the ξ value increases and finally the ϑ value for both methods becomes stable for a ξ value above 10^6.

This indicates that ξ value is large enough to realize the worst case WEG uncertainty that system can be alleviated. As a result, it can be concluded that it is of great

importance to select an appropriate ξ value to accurately represent the worst case WEG uncertainty while finding optimum IC and OC.

Also, as shown in these tables, the impact of ξ on the value of ϑ for CTM is higher than DTM, accordingly, the CTM can provide more robust solution than DTM. The reason is that the higher ξ value implies the more storage capacity and as mentioned before the number of FA-ESS and their capacity in the CTM will be higher than the other one.

***B. Optimal Allocation of FA-ESS, for DTM and CTM, versus Investment Budget*:** The impact of the investment budget (Π) on optimal allocation of FA-ESS for DTM and CTM is illustrated in Tables IV and V. In these tables, the weighting parameter of uncertainty is fixed to 10^6 while the value of Π is changed progressively. Interesting insights can be inferred from these tables.

(i) As expected, it can be observed that as the Π value grows, the IC increases while additional FA-ESSs are installed to relieve transmission congestion and manage the variability of WEG. An important result is that the investment decisions become stable for DTM and CTM once the number of FA-ESSs reaches 5 and 6, respectively.

Comparing the results for DTM and CTM, it can be observed the storage capacity and number of FA-ESSs, for $\Pi \leq 10$ M$, are the same for both methods, while, for $\Pi >$ 10 M$ the storage capacity and number of FA-ESSs for the CTM have been more increased. As a result, it is concluded that the CTM has a great capability to utilize more storage capacity and the number of FA-ESS in power systems.

(ii) The OC and the total cost (Φ) are not a linear function of Π value. The results of this exhaustive search indicate the increase of Π value may decrease the OC, Φ. Noted that, the minimum OC for CTM is obtained when Π is equal to 20 M$. Similarly, the minimum OC for DTM is achieved when Π is equal to 10 M$. The OC and Φ for Π = 0 M$ (or without any FA-ESS) is studied here.

The OC and Φ of the proposed problem using the proposed CTM are more than the DTM. The increase in the OC and Φ for the proposed CTM is expected because the method dispatches more energy to supply the continuous-time variations of load and WEG in the operation stage. But, once $\Pi > 0$ M$, the OC for the proposed CTM has been more decreased than the DTM. Because, the DTM does not capture ultimate storage capacity, power charging/discharging and very fast ramping of FA-ESSs to supply the continuous time load and WEG variations while the proposed CTM explicitly captures continuous-time energy storage capacity, power charging/ discharging and very fast ramping of the FA-ESSs. Thus, for Π = 20 M$, the OC and Φ for the proposed CTM are in the least values.

TABLE II: Optimal allocation of FA-ESS for DTM versus weighting parameter of uncertainty; IC≤20 M$.

ξ	Number of FA-ESSs	Built FA-ESSs Bus-(Capacity (MWh))	IC (M$)	OC (M$)	Φ (M$)	ϑ
0	3	1-(133), 3-(1000), 8-(54)	5.9	336.3	342.2	0.000
10^2	3	1-(133), 3-(1000), 7-(54)	5.9	336.3	342.2	0.074
10^4	4	3-(1000), 7-(20), 8-(62.24), 9-(163.02)	6.3	360.1	366.4	0.113
10^6	5	3-(952.4), 4-(179.7), 9-(1000), 11-(531.6), 12-(1000)	18.3	593.5	611.8	0.465
10^8	5	3-(952.4), 4-(179.7), 9-(1000), 11-(531.6), 12-(1000)	18.3	593.5	611.8	0.465

TABLE III: Optimal allocation of FA-ESS for CTM versus weighting parameter of uncertainty; IC≤20 M$.

ξ	Number of FA-ESSs	Built FA-ESSs Bus-(Capacity (MWh))	IC (M$)	OC (M$)	Φ (M$)	ϑ
0	3	3-(1000), 8-(617.4), 9-(288)	9.5	280.8	290.3	0.000
10^2	3	3-(1000), 8-(617.4), 9-(288)	9.5	280.8	290.3	0.081
10^4	3	3-(1000), 8-(544.9), 9-(387.1)	9.6	281.8	291.4	0.129
10^6	6	3-(966.8), 4-(179.8), 8-(378.5) 9-(1000), 12-(1000), 13-(513.3)	19.8	366.9	386.7	0.528
10^8	6	3-(966.8), 4-(179.8), 8-(378.5) 9-(1000), 12-(1000), 13-(513.3)	19.8	366.9	386.7	0.528

TABLE IV: Optimal allocation of FA-ESS for DTM versus IC; $\xi=10^6$.

Π (M$)	Number of FA-ESSs	Built FA-ESSs Bus-(Capacity (MWh))	IC (M$)	OC (M$)	Φ (M$)	ϑ
0	0	-	0	459.6	459.6	0.205
1	1	3-(200)	1	439.7	440.7	0.232
5	2	3-(351.8), 9-(648.2)	5	455.1	460.1	0.327
10	4	3-(492.3), 4-(279.6), 9-(1000), 12-(228.1)	10	525.6	535.6	0.428
20	5	3-(952.4), 4-(179.7), 9-(1000), 11-(531.6), 12-(1000)	18.3	593.5	611.8	0.465
40	5	3-(952.4), 4-(179.7), 9-(1000), 11-(531.6), 12-(1000)	18.3	593.5	611.8	0.465

TABLE V: Optimal allocation of FA-ESS for CTM versus IC; $\xi=10^6$.

Π (M$)	Number of FA-ESSs	Built FA-ESSs Bus-(Capacity (MWh))	IC(M$)	OC (M$)	Φ (M$)	ϑ
0	0	-	0	461.6	461.6	0.208
1	1	3-(200)	1	432.7	433.7	0.234
5	2	3-(351.8), 9-(648.2)	2	416.1	421.1	0.338
10	4	3-(492.3), 4-(279.6), 9-(1000), 12-(228.1)	10	436.2	446.3	0.448
20	6	3-(966.8), 4-(179.8), 8-(378.5) 9-(1000), 12-(1000), 13-(513.3)	19.8	366.9	386.7	0.528
40	6	3-(966.8), 4-(179.8), 8-(378.5) 9-(1000), 12-(1000), 13-(513.3)	19.8	366.9	386.7	0.528

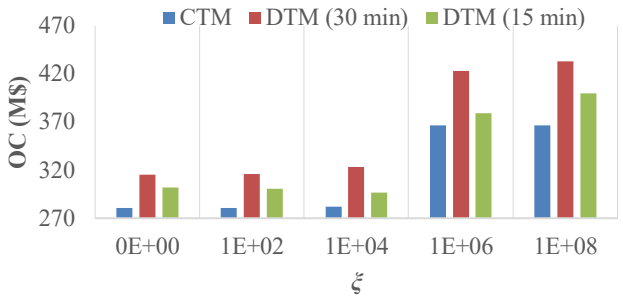

Fig.6. The OC for CTM and DTM with different sub-hourly intervals.

(iii) Simulation results justify increasing the values of Π from 0 M$ to 20 M$ results in more robust solutions withstanding more diverse realization of uncertain WEGs. Two obstacles to increase the value of ϑ are transmission line congestion, i.e., congestion at line 3-24, and lack of ramping requirement to mitigate WEG uncertainty. For example, for this test system as shown in Tables IV and V, the congestion at line 3-24 (with low capacity) is mitigated by installing an FA-ESS at bus 3, and the ramping problem is solved by installation of an FA-ESS with adequate storage capacity at bus 9 or other buses. Besides, as can be seen in Tables IV and V, the value of ϑ is increased for both methods once Π varies from 0 M$ to 20 M$. Nevertheless, as shown in these tables, the ϑ value for the proposed CTM is more increased than DTM. This is expected, because by increasing the value of ϑ, the large amount of ramp capability is necessary to cover the wind generation uncertainty in the real-time operation. As mentioned earlier, the CTM has more ability to provide sufficient ramp capacity in power systems than DTM. These results confirmed that with the CTM compared to DTM can obtain more robust solution (higher ϑ value) with the lower total costs.

C. Compare DTM with Different Sub-hourly Intervals with CTM:

In order to evaluate the performance of our proposed CTM in different weighting parameter of uncertainty (ξ), we repeated the OC in Fig. 6 for the CTM and also added the OC results obtained from the DTM with 30 min and 15 min sub-hourly intervals. We assume that the total investment budget (Π) is 20 M$. We observe from Fig. 6 that our proposed CTM outperforms the other two DTMs in terms of total operation cost reduction, even compared to the 15 min sub-hourly interval solution.

VII. Conclusions

This paper presents an interval based robust optimization model based on continuous/discrete time method to investigate the best allocation of FA-ESS on the transmission network in the presence of the high penetration of wind energy generation. The FA-ESS is supposed to provide fast ramping capability to mitigate wind power uncertainty. The proposed problem based on CTM and DTM allows finding the best allocation of FA-ESSs among different buses of the transmission network in order to achieve specific objectives. Considering the theoretical properties of the proposed model and the results of the case studies carried out, the conclusions below are in order:

- The obtained results highlight the significance of implementing the CTM in placement problems. Consequently, in order to compensate for power mismatches caused by wind forecast errors, an enough ramping capacity should be considered in the system. However, it is noted that despite the availability of ramping capacity in the system, due to lack of ability in the DTM, it cannot be utilized as addressed in this paper.
- The obtained results from the 24-bus test system illustrate that sizing and sitting of FA-ESS highly depend on weighting parameter of the uncertainty as well as the investment budget availability.
- The results demonstrate the superiority of CTM compared to DTM to present more robust solution (higher ϑ value) with lower total costs.
- The results pinpoint the necessity of an accurate time method for economically proper system operation.
- The optimal sizing and sitting of the FA-ESS should be determined based on the CTM rather than DTM.
- The proposed CTM is more capable than DTM in terms of finding the worst case of wind energy uncertainty and controlling it.

Future study should address the best combination, in term of number, size and location for allocation of FA-ESSs.

References

[1] Global Wind Energy Council (GWEC), Global Wind Report: Annual Market Update 2011 [Online]. Available: http://gwec.net/wp-content/uploads/2012/06/Annual_report_2011_lowres.pdf.

[2] N. Zhang *et al.*, "Planning pumped storage capacity for wind power integration," *IEEE Transactions on Sustainable Energy,* vol. 4, no. 2, pp. 393-401, 2013.

[3] L. Fiorini, G. A. Pagani, P. Pelacchi, D. Poli, and M. Aiello, "Sizing and siting of large-scale batteries in transmission grids to optimize the use of renewables," *IEEE Journal on Emerging and Selected Topics in Circuits and Systems,* vol. 7, no. 2, pp. 285-294, 2017.

[4] M. Aien, A. Hajebrahimi, and M. Fotuhi-Firuzabad, "A comprehensive review on uncertainty modeling techniques in power system studies," *Renewable and Sustainable Energy Reviews,* vol. 57, pp. 1077-1089, 2016.

[5] A. J. Conejo, Y. Cheng, N. Zhang, and C. Kang, "Long-term coordination of transmission and storage to integrate wind power," *CSEE Journal of Power and Energy Systems,* vol. 3, no. 1, pp. 36-43, 2017.

[6] D. Bertsimas, E. Litvinov, X. A. Sun, J. Zhao, and T. Zheng, "Adaptive robust optimization for the security constrained unit commitment problem," *IEEE Transactions on Power Systems,* vol. 28, no. 1, pp. 52-63, 2013.

[7] A. Nikoobakht, J. Aghaei, T. Niknam, V. Vahidinasab, H. Farahmand, and M. Korpås, "Towards robust OPF solution strategy for the future AC/DC grids: case of VSC-HVDC-connected offshore wind farms," *IET Renewable Power Generation,* vol. 12, no. 6, pp. 691-701, 2018.

[8] X. Zhang and A. J. Conejo, "Coordinated Investment in Transmission and Storage Systems Representing Long-and Short-term Uncertainty," *IEEE Transactions on Power Systems,* 2018.

[9] S. Wogrin and D. F. Gayme, "Optimizing storage siting, sizing, and technology portfolios in transmission-constrained networks," *IEEE Transactions on Power Systems,* vol. 30, no. 6, pp. 3304-3313, 2015.

[10] H. V. Haghi and S. Lotfifard, "Spatiotemporal modeling of wind generation for optimal energy storage sizing," *IEEE Transactions on Sustainable Energy,* vol. 6, no. 1, pp. 113-121, 2015.

[11] T. Qiu, B. Xu, Y. Wang, Y. Dvorkin, and D. S. Kirschen, "Stochastic multistage coplanning of transmission expansion and energy storage," *IEEE Transactions on Power Systems,* vol. 32, no. 1, pp. 643-651, 2017.

[12] S. Dehghan and N. Amjady, "Robust transmission and energy storage expansion planning in wind farm-integrated power systems considering transmission switching," *IEEE Transactions on Sustainable Energy,* vol. 7, no. 2, pp. 765-774, 2016.

[13] Y. Zhang, S. Zhu, and A. Chowdhury, "Reliability modeling and control schemes of composite energy storage and wind generation

system with adequate transmission upgrades," *IEEE transactions on sustainable energy,* vol. 2, no. 4, pp. 520-526, 2011.

[14] R. A. Jabr, I. Džafić, and B. C. Pal, "Robust optimization of storage investment on transmission networks," *IEEE Transactions on Power Systems,* vol. 30, no. 1, pp. 531-539, 2015.

[15] J. Zhan, W. Liu, and C. Chung, "Stochastic Transmission Expansion Planning Considering Uncertain Dynamic Thermal Rating of Overhead Lines," *IEEE Transactions on Power Systems,* vol. 34, no. 1, pp. 432-443, 2019.

[16] R. A. Jabr, "Robust transmission network expansion planning with uncertain renewable generation and loads," *IEEE Transactions on Power Systems,* vol. 28, no. 4, pp. 4558-4567, 2013.

[17] C. Ruiz and A. J. Conejo, "Robust transmission expansion planning," *European Journal of Operational Research,* vol. 242, no. 2, pp. 390-401, 2015.

[18] N. Navid and G. Rosenwald, "Ramp capability product design for MISO markets," *Market Development and Analysis,* 2013.

[19] S. Wang, G. Geng, and Q. Jiang, "Robust Co-Planning of Energy Storage and Transmission Line with Mixed Integer Recourse," *IEEE Transactions on Power Systems,* 2019.

[20] Y. J. A. Zhang, C. Zhao, W. Tang, and S. H. Low, "Profit-maximizing planning and control of battery energy storage systems for primary frequency control," *IEEE Transactions on Smart Grid,* vol. 9, no. 2, pp. 712-723, 2016.

[21] J. Li *et al.*, "Robust coordinated transmission and generation expansion planning considering ramping requirements and construction periods," *IEEE Transactions on Power Systems,* vol. 33, no. 1, pp. 268-280, 2017.

[22] F. Zhang *et al.*, "Battery ESS planning for wind smoothing via variable-interval reference modulation and self-adaptive SOC control strategy," *IEEE Transactions on Sustainable Energy,* vol. 8, no. 2, pp. 695-707, 2016.

[23] A. Nikoobakht, J. Aghaei, M. Shafie-Khah, and J. P. Catalão, "Assessing increased flexibility of energy storage and demand response to accommodate a high penetration of renewable energy sources," *IEEE Transactions on Sustainable Energy,* vol. 10, no. 2, pp. 659-669, 2019.

[24] X. Chen, J. Tan, Z. Liu, and J. Xie, "Approximation of functions by a new family of generalized Bernstein operators," *Journal of Mathematical Analysis and Applications,* vol. 450, no. 1, pp. 244-261, 2017.

[25] R. T. Force, "The IEEE reliability test system-1996," *IEEE Trans. Power Syst,* vol. 14, no. 3, pp. 1010-1020, 1999.

[26] National Renewable Energy Laboratory (NERL). Wind integration datasets. [Online]. Available: http://www.nrel.gov/grid/wind-integrationdata.html/.

[27] A. Ahmadi-Khatir, A. J. Conejo, and R. Cherkaoui, "Multi-area unit scheduling and reserve allocation under wind power uncertainty," *IEEE Transactions on power systems,* vol. 29, no. 4, pp. 1701-1710, 2013.